Embedded Actuation for Shape-Adaptive Origami

Steven W. Grey, Fabrizio Scarpa, Mark Schenk
Bristol Composites Institute
University of Bristol
Bristol, BS8 1TR
United Kingdom
email: m.schenk@bristol.ac.uk

Origami-inspired approaches to deployable or morphing structures have received significant interest. For such applications the shape of the origami structure must be actively controlled. We propose a distributed network of embedded actuators which open/close individual folds, and present a methodology for selecting the positions of these actuators. The deformed shape of the origami structure is tracked throughout its actuation using local curvatures derived from discrete differential geometry. A Genetic Algorithm (GA) is used to select an actuation configuration, which minimises the number of actuators or input energy required to achieve a target shape. The methodology is applied to both a deployed and twisted Miura-ori sheet. The results show that designing a rigidly foldable pattern to achieve shape-adaptivity does not always minimise the number of actuators or input energy required to reach the target geometry.

1 Introduction

The ability to transform from a flat sheet to a three-dimensional shape has led to significant interest in the use of origami-inspired solutions to deployable [1, 2] and morphing [3] engineering problems. Consideration of how such origami-inspired systems will be actuated to achieve the intended change in configuration must be integral to the design process.

One common approach in self-folding origami is to use an environmental stimulus, which affects all folds simultaneously, to trigger a predefined motion [4]. Alternatively, each fold can be actuated independently to achieve complex three-dimensional shapes; for example, the 'Stanford bunny' actuated using shape memory alloy folds [5]. Such patterns have a large number of degrees of freedom (DOFs); therefore, a large number of actuators is required to successfully control them. Alternatively, the inherent kinematics of origami can be exploited by selecting patterns with a single DOF, such as the Miura-ori, so that a single actuator can control the shape of the entire structure. This approach would be ideal for systems required to follow a single deformation path, such as deployable structures, minimising the cost and complexity of the actuation system [6,7,8]. However, this relies on the rigid origami assumption that the folds are perfect hinges and the facets — material between the folds — are infinitely stiff. In physical systems, the folds have a torsional stiffness and the facets can deform, meaning that a pattern such as the Miura-ori no longer has a single DOF and the effect of a single actuator decays instead of propagating uniformly across the entire structure [9]. This has the implication that the number and position of actuators influences the response of the structure, meaning that a distributed network of embedded actuators is essential.

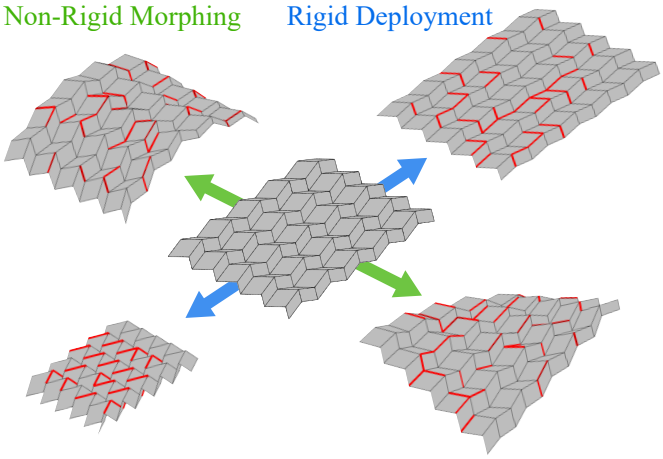

Fig. 1: Miura-ori sheets can be deployed (according to its rigid-origami kinematics) or morphed (requiring facet deformations) using a distributed network of actuators — here represented by the rotation of highlighted fold lines

On the other hand, the increase in DOFs introduced by facet bending does enable morphing of the origami structure into shapes not permissible by rigid origami. What is more, re-configurable origami can be designed to exploit multi-stabilities to maintain the new shape without additional energy [3, 10, 11]. By considering both deployment and morphing, we utilise the entire configuration space of actuated origami, as visualised in Figure 1. This could be extended to the design of a system where the same distributed network of

embedded actuators could be used to reconfigure the structure from one shape to another, similar to the 'programmable matter' proposed by Hawkes *et al.* [12].

Physical realisation of these actuators in origami structures could take many forms, from tendons [13] or magnets [14] pulling points together, to smart materials such as shape memory polymers or alloys providing a moment along the folds [15, 16]. The focus of this paper is not to faithfully reproduce any one of these methods, but instead to explore a methodology by which the optimal positions of these actuators can be selected. Therefore, we idealise an actuation as a pure rotation which is uniform along the length of a fold. One potential combination of such actuators, to achieve the least error in deployment or morphing, is to place an independently controlled actuator on every fold. However, each actuator has an associated mass, cost and power usage — all of which should be minimised. Therefore, we develop a methodology to determine the minimum number of actuators and their optimal locations in an origami-inspired deployable or morphing structure to achieve the desired target shape. We focus our investigation on open loop control, *i.e.* no embedded sensing of the deformed configuration.

In Section 2 we propose a novel methodology for quantifying the quality-of-fit of the actuated origami compared to the target surface and show how a Genetic Algorithm (GA) can be used to design the positions of the actuators. The Miura-ori pattern is here used as a case study; however, the methodology is not limited to this pattern and could be applied to a wide range of origami structures. Next, Sections 3 and 4 show examples of optimising the position and number of actuators in order to achieve deployment or morphing in a Miura-ori sheet, using the fewest actuators or the least amount of energy.

2 Methods

The following section outlines a methodology for modelling an origami structure and tracking its shape throughout an actuation. This enables the placement of actuators to achieve a desired target shape. The number of combinations of actuated folds, even in relatively small Miura-ori sheets, presents a challenge for searching the design space, and a Genetic Algorithm (GA) is selected to address this.

2.1 Actuator Placement & Modelling

Many rigid origami patterns consist of a network of quadrilateral facets connected by folds, resulting in a single degree of freedom. In physical systems the folds and facets have a finite stiffness and the deployments do not always follow the the kinematics predicted by rigid origami. Triangulating the facets by including pseudo-folds, and assigning a torsional stiffness to the folds and pseudo-folds, is a first approximation to model non-rigid foldable motions [17, 18].

The pseudo-folds introduce finite additional degrees of freedom, nonetheless allowing the state of the complete origami structure to be defined using a subset of the folds. One approach is to define the shape of an entire Miura-ori sheet by the angles of the folds and pseudo-folds on the boundary [19]. Physical implementation would be challenging as controlling the angle of the pseudo-folds along the short diagonals of the facets would require bending the facets themselves. Alternatively, starting from a selected zig-zag pattern of folds, the shape of the entire sheet can be algorithmically propagated [20]. Neglecting the in-plane facet deformations is a limitation of both methods, as these may cause unexpected physical responses which drive the final actuated shape [9].

In order to accurately capture both the in-plane and out-of-plane facet deformations, the finite element analysis (FEA) package ABAQUS is used. The facets are modelled with S4R shell elements (a 10×10 mesh per facet) and the folds with CONN3D2 connector elements between coincident nodes of adjoining facets. This models the origami structure as a series of shells connected by hinges with a torsional stiffness. The fold angles at these connection points are defined as the angles between tangents of both facets at the point they meet. An actuation is produced by enforcing a rotation in the CONN3D2 elements, where the energy required is given by the product of the reaction moment and hinge rotation at the element. Material properties represent polyethylene terephthalate (PET) film used for prototyping, with a Young's modulus, Poisson's ratio and thickness of 3.2 GPa, 0.43, and 200 μm respectively. The torsional stiffness for the folds is 0.05 N/rad. The initial configuration of the Miura-ori is given as $a = b = 30$ mm, $\alpha = 60^\circ$ and $\psi_0 = 120^\circ$, where a, b, α and ψ are defined in Figure 2. Unless otherwise stated these properties and geometry are used for all subsequent models in this paper.

To maintain compatibility between folds at each vertex, the magnitude of the actuated rotation on each of the folds is calculated from the rigid origami kinematics of the Miura-ori. The relationship between the ψ and β folds, as defined

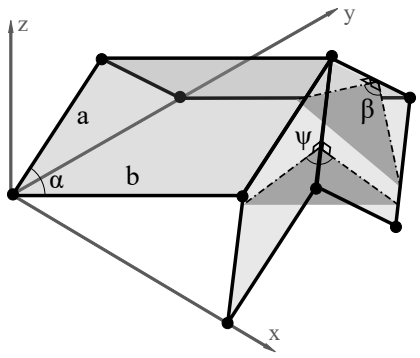

Fig. 2: Miura-ori unit cell and its geometric parameters. Fold angles β and ψ are actuated to achieve deployment or morphing of the unit cell

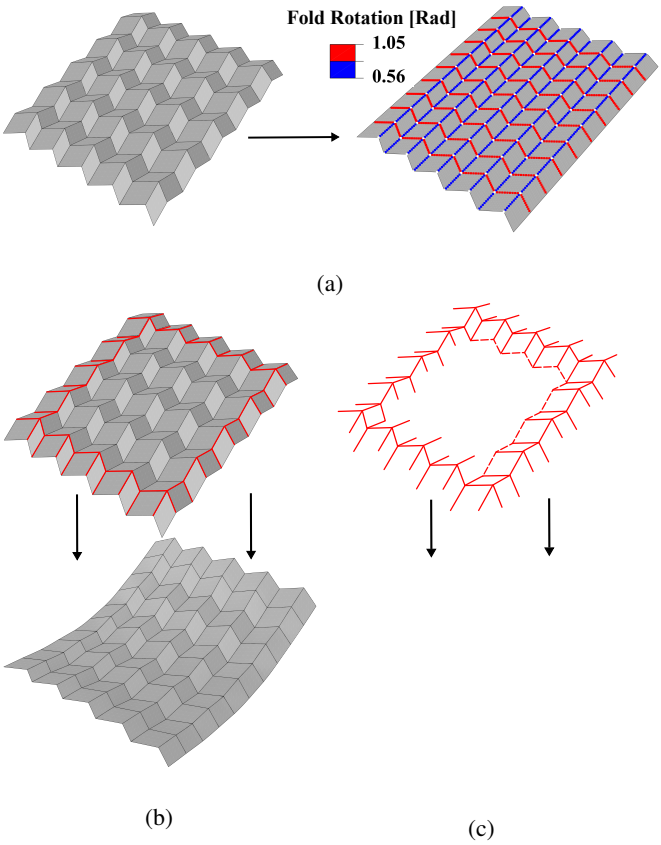

Fig. 3: (a) Actuating every fold in a Miura-ori sheet leads to a perfectly deployed sheet; colours indicate magnitude of fold rotation. Controlling a subset of folds using identical actuation inputs does not lead to a uniform deployment due to facet bending. A symmetric actuation pattern along the perimeter leads to a saddle shape (b); a slightly asymmetric pattern produces a twisted shape (c); actuated folds are highlighted

in Figure 2, is provided by Equation 1 [21, 22].

$$\sin\left(\frac{\psi}{2}\right) = \frac{\cos(\alpha)\sin\left(\frac{\beta}{2}\right)}{\sqrt{1-\left(\sin(\alpha)\sin\left(\frac{\beta}{2}\right)\right)^2}} \tag{1}$$

Figure 3 illustrates the importance of actuator positioning on the resulting deployed shape: two different actuator combinations, both along the boundary of a 5×5 Miura-ori sheet, share the same actuated fold rotation as in a rigid origami deployment. However, facet deformations result in different final configurations for the different actuator placements. For example, selecting an asymmetric pattern of actuators leads to a twisted sheet; see Figure 3c. This highlights how, when modelling an actuated origami design it is crucial to track its shape throughout the deployment to ensure it can adequately achieve its intended target.

2.2 Quantifying Quality of Fit

An intuitive method of quantifying the quality of fit is to compare geometric parameters defining the origami in the actuated sheet to those in the target configuration, such as fold angle [24] or nodal positions [25]. Alternatively, when designing for a specific application, a functional parameter could be used to define the quality of fit; for example, the exposed area of photo-voltaic cells in a solar array [26] or the thermal performance of a radiator [27].

One commonly used method for comparing deformed and target shapes is the Hausdorff distance [3,28,29,11]. Let both the target surface, A, and the actuated surface, B, be discretised into a set of points. The distance from all points in A to their nearest point on B can be found; likewise, the distance from all the points in B to their closest point on A can be determined. The Hausdorff distance is the maximum from either of these two sets of distances. However, this approach is sensitive to a single poorly fitting point describing the quality of fit of the entire structure. Using the root mean square error (RMSE) of the Euclidian normal distance to the target surface [30] could reduce the sensitivity to outliers, but this comes at the cost of additional computational effort. Curvature has been used previously in the generation of fold patterns designed to fit to a target surface by homogenising the Miura-ori tessellation into a smooth surface [20, 31]. However, to calculate the curvature two assumptions are needed: first, the region over which the curvature is calculated must be sufficiently larger than the size of a single unit cell; and second, the radius of curvature must be sufficiently larger than the region over which the curvature is calculated. Essentially, this technique is limited to large tessellations with small curvatures, relative to their size, and so could not be applied to the examples shown in Figure 1.

We propose using an alternative method of defining the curvature across an origami structure using principles from discrete differential geometry [23]. First, the vertices on the top or bottom of the Miura-ori sheet, shown for the top only in Figure 4, are triangulated to form a discrete surface. Next, the curvatures at the vertices which are completely surrounded by triangles are calculated, starting with the Gaussian curvature:

$$\kappa_G(\mathbf{x_i}) = \frac{2\pi - \sum_{j=1}^{N_v}\theta_i}{A_v} \tag{2}$$

where N_v is the number of vertices surrounding the vertex at coordinate $\mathbf{x_i}$ (*i.e.* six for the Miura-ori), and the Voronoi area, A_v is defined as

$$A_v = \frac{1}{8}\sum_{j=1}^{N_v}(\cot(\gamma_{ij})+\cot(\phi_{ij}))\|\mathbf{x_i}-\mathbf{x_j}\|^2 \tag{3}$$

where angles θ_i, γ_{ij} and ϕ_{ij} are defined in Figure 5. Note, this formulation is only valid where these angles are acute; however, this is sufficient for the geometries and deformations analysed in this paper. Further details are found in Meyer *et al.* [23].

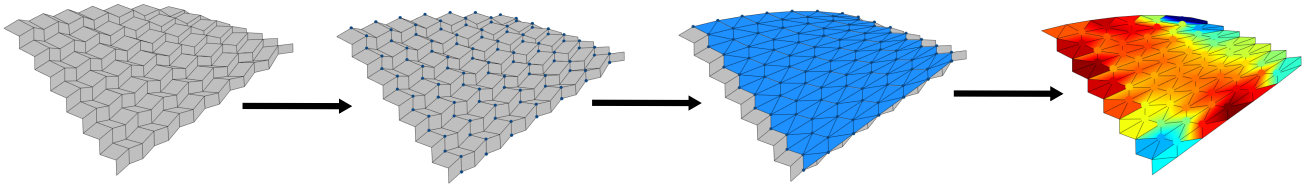

Fig. 4: Calculation of curvatures across a deformed Miura-ori sheet: the vertices on the upper surface form a triangulated surface; the mean and Gaussian curvatures are calculated using discrete differential geometry [23]. Finding the curvature of the lower surface follows the same process with the corresponding vertices

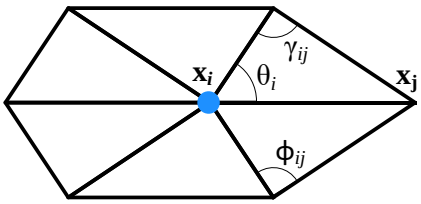

Fig. 5: Definition of geometric terms used in the calculation of the curvature at point i on a triangulated surface

The Gaussian curvature does not provide a complete picture of the overall shape, as a flat sheet and singly curved configuration will give the same result. The mean curvature, κ_H is given as:

$$\kappa_H = \frac{1}{4A_v}\left\| \sum_{j=1}^{N_v} (\cot(\gamma_{ij}) + \cot(\phi_{ij}))(\mathbf{x_i} - \mathbf{x_j}) \right\|. \quad (4)$$

Combining these two curvatures allows for a unique description of the shape of any surface representing the upper or lower vertices. Equation 5 is used to obtain the principal curvatures, κ_1 and κ_2.

$$\kappa_1, \kappa_2 = \kappa_H \pm \sqrt{\kappa_H^2 - \kappa_G} \quad (5)$$

Utilising the principal curvatures as metric also removes the need to account for rigid body rotations between the actuated model compared to the target shape. Furthermore, the metric allows for a good fit between actuated and target geometry, even if the fold angles do not match; this is useful for morphing structures where the fold stiffness is comparatively high compared to the facet stiffness.

However, in the case of a Miura-ori sheet deploying from a partly folded state to a flattened configuration, where the initial surface curvatures are the same as the targets, an additional parameter is required to define the error. The RMSE of all the fold angles in the sheet is used for this, as fold rotation is an ABAQUS\Standard output and so minimises computational cost compared to computing other angles or the distance between the planes representing the upper and lower vertices.

2.3 Optimisation

Assuming the magnitude of actuation required for deployment is known, the most robust method of finding the optimal place of actuators would be to test every possible combination. However, even for relatively small origami structures, the number of possible combinations of folds which could be actuated becomes impractically large. For a Miura-ori sheet with n and m cells in the x and y directions, defined in Figure 2, the total number of folds F is given by

$$F = 4mn + 2m(n-1) + 2n(m-1). \quad (6)$$

If any of these folds can either be actuated or not, the total number of combinations of actuators C_a is given by

$$C_a = 2^F - 1 \quad (7)$$

where the case of actuating no folds is excluded. This exponential rise of actuators has severe implications. Even for a small Miura-ori sheet with $n = m = 3$, this results in $O\left(10^{18}\right)$ possible actuator combinations! Clearly, for any practically usable system an optimisation algorithm is essential to selectively probe this design space and select a high-performing actuator combination.

Ideally, any optimisation algorithm and constraints we choose should be verified against an exhaustive search of a similar domain; therefore, we aim to reduce this design space to a practical size. First, we pair the actuation of ψ-folds — forming chevrons pointing in the positive y-direction — and β-folds — forming chevrons pointing in the positive z-direction — and actuate both or neither; this halves the order of magnitude for C_a. Next, the design space is further reduced by only actuating either ψ or β-folds. For the 3×3 Miura-ori, this leaves a more achievable 32,767 combinations.

Previous explorations of the structural optimisation of origami focus on tuning the fold stiffness across the structure to minimise the force required at a given node to produce a defined displacement [32]. This formulation results in a binary pattern of high and low values representing fold and facet bending stiffness. This non-convex problem required a global optimisation algorithm to regularly produce an optimal solution [33]. Similarly, we employ a Genetic Algorithm (GA) (as implemented in the MATLAB 'Global Op-

timization Toolbox' [34]) to find the optimal actuator combinations, as it handles the discrete nature of the actuator placement to achieve deployment.

A constraint is applied to the GA, penalising solutions failing to satisfy a specified tolerance of the quality of fit

$$f = \frac{1}{N_c}\left(\left(\frac{\kappa_{1,\mathrm{RMSE}}}{\kappa_{1,tol}}\right)^p + \left(\frac{\kappa_{2,\mathrm{RMSE}}}{\kappa_{2,tol}}\right)^p + \left(\frac{\theta_{\mathrm{RMSE}}}{\theta_{tol}}\right)^p\right) + 1 \tag{8}$$

which has a value of $f \approx 1$ for outputs within the tolerance and exponentially increases outside the defined tolerance, controlled by exponent p. Parameters $\kappa_{1,\mathrm{RMSE}}$, $\kappa_{2,\mathrm{RMSE}}$, and θ_{RMSE} represent the RMSE in the principal curvatures and the fold angles respectively; $\kappa_{1,tol}$, $\kappa_{2,tol}$, and θ_{tol} are the corresponding tolerances. The total number of constraints N_c, three in this case, can be varied depending on which terms are important for a given application. It is the product of f and the parameter to be minimised, either input energy or number of actuators, which forms the objective function in the GA.

The selection of the specific parameter to be minimised depends on the intended application. If the system is energy limited then minimising the required actuation energy would be prudent; likewise for mass limited systems minimising the number of actuators is sensible. For a real engineering application a weighted combination of both of these factors is most likely to drive the design. However, the objective of our optimisation is to minimise either the input energy or the total number of actuators required to achieve the desired deployment or morphing within the target geometric tolerance, in order to gain insight into the difference between these objectives.

This could take one of two forms: first, selecting which folds should be actuated, where the size of the actuation at each fold is predetermined; or second, selecting how much a predetermined set of actuators should be actuated. The former is applied to patterns which could follow a rigid origami path from their initial to final states; for instance, the deployment of a Miura-ori sheet, where the desired direction and magnitude of fold rotations are known. The latter is useful for non-rigid deformations, for example a twisting of a Miura-ori sheet, where the direction and magnitude of the actuation are unknown.

3 Planar Deployment

Using this methodology we explore how the positioning of rotational actuators in a 3×3 Miura-ori sheet affects its deployment to a state where the ψ-folds are 90% of the way from the initial state to a fully flat configuration, with the objective of minimising either the input energy or the number of actuators required. Avoiding the fully flattened state limits the possibility of pop-through defects [10] occurring; any actuator combinations which did elicit this response are left out of the database. Building an exhaustive database of all combinations of actuated pairs of ψ-folds and β-folds and their performance enables both the verification of the GA and provides insight into the effect of actuating these two different types of folds.

Consider first the minimisation of the number of actuators, as shown in Figure 6a. It is immediately clear that actuating a combination of ψ-folds is more effective than β-folds to achieve deployment. Using the GA to probe the smallest number of actuators required to achieve the same target tolerances in a 5×5 Miura-ori sheet, where now any combination of ψ-fold and β-fold pairs can be selected, also returns a set containing only pairs of ψ-folds; see Figure 7. This result could be due to the kinematics of the Miura-ori: first, the β-folds are all parallel, and so they rely on the vertex kinematics to propagate their actuation in both x- and y-directions; second, the ψ-folds have to open further to reach a flattened state, thereby imparting more energy for a given number of actuators. This is reflected if we instead consider the actuator configuration with minimum energy requirement, see Figure 6b, which shows it is now the pairs of β-folds which yield a more effective combination. A realistic scenario could be a trade-off between these two cases; there would be constraints on the energy available and each actuator installed would introduce additional cost and mass.

In order to populate the reference database and perform the actuator placement optimisation, the sheet target geometry, the expected geometric tolerances and optimisation constraint parameters must be defined.

For the planar deployment of a Miura-ori sheet considered here, defining the target geometry is straightforward: both principal curvatures are equal to zero at every point, and all fold angles β and ψ across the sheet are defined by the unit cell kinematics. However, defining the tolerances of these parameters is dependent on the specific application for which the system is designed. In this work a tolerance of $\kappa_{tol} = 5\,\mathrm{mm}^{-1}$ for each of the principal curvatures and $\theta_{tol} = 0.5$ radians for the fold angles is used. For the selected PET material properties, these settings give a good range of combinations providing shapes both within and outside of the tolerance. This allows us to both demonstrate the efficacy of our process to characterise the shape of the origami throughout the folding process, and to investigate the advantages and disadvantages of different sets of actuators.

Selection of the parameter p, which controls the exponential increase of the penalty function in Equation 8, also affects the optimal solutions. Larger values of p apply a greater penalty to combinations of actuators resulting in curvatures or fold angles outside the tolerances. However, an excessively large value for p can cause a GA to become less reliable at tending towards the optimal combination. Therefore, a sensitivity analysis is used to select a value for p. For the minimisation of actuator number and actuation energy, 100 GA optimisations were run to find the optimal solutions for either ψ- or β-fold pairs. These were compared with the known optimal combinations from the databases to quantify the accuracy of the GAs. Table 1 shows the number of times the GA resulted in the optimal combination and the maximum error between the GA result and the known optimum, which leads to three conclusions. First, this sensitivity analysis verifies the use of a GA to find a high-performing

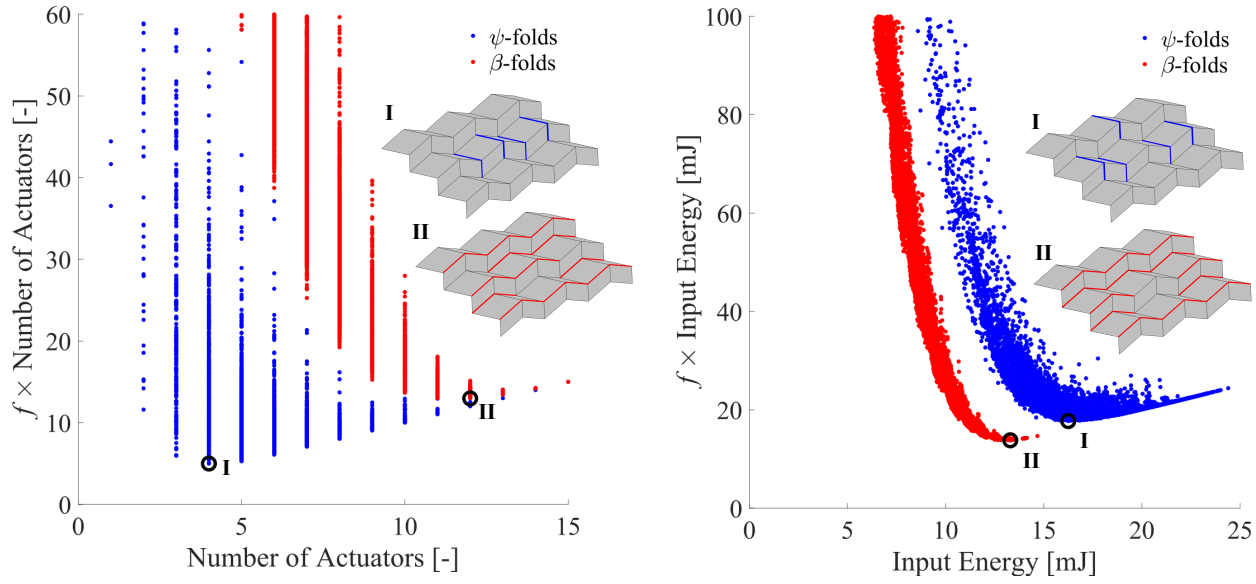

(a) (b)

Fig. 6: An exhaustive search of all possible combinations of ψ (blue) and β (red) fold pair actuators targeting the deployment of a 3×3 Miura-ori sheet. A penalty function, defined in Equation 8, using curvature tolerances of $5\,\mathrm{mm}^{-1}$, a fold angle tolerance of 0.5 rad, and an exponential factor $p = 10$, is applied to the results and used to (a) minimise the total number of actuators and (b) minimise the actuation energy. Inset are the optimal actuation configurations for both sets of actuation

combination of actuators; for $p = 10$ and $p = 25$ the optimal combination is the most common result and the maximum error is not more than a few percent. Second, the final column in Table 1 highlights how, despite not always being the best solution, selecting a combination of actuators which is symmetric in the plane of symmetry of the Miura-ori sheet still reliably results in a high quality configuration. Limiting the design space to symmetrically-placed pairs of actuated folds would reduce it by an order of magnitude for a 3×3 Miura-ori sheet, and 12 orders of magnitude for a 5×5 Miura-ori sheet. Finally, a value of $p = 10$ provides a minimum error when aggregated across all four scenarios, therefore we use this to generate the results in Figures 6 and 7; however, the results do not change significantly for either $p = 5$ or $p = 25$.

4 Non-Planar Morphing and Deployment

In exploring the transformation of origami structures, we now shift our focus from deploying a rigid-foldable Miura-ori sheet, to morphing from a partly-deployed state to another three-dimensional shape. Specifically, we investigate the twisting of a 5×5 Miura-ori sheet as a simple but representative morphed configuration. The target twisted shape is defined by displacing the central vertices of the bottom-left and top-right unit cells by $+2.5H$ and the central vertices of the bottom-right and top-left unit cells by $-2.5H$ in the z-direction; see Figure 8a. After simulating the deformed shape using FEA, the fold rotations are extracted and the principal curvatures at the vertices on the lower surface are calculated.

For the planar deployment in Section 3, the required actuation magnitudes are known from the unit cell kinematics. For morphing, the measured fold rotations, shown in Figure 8a, are used as a starting point for determining the required actuation magnitude to achieve the target twisted shape. Examination of the fold rotations reveals that it is no longer possible to pair folds at each vertex or consider only symmetric actuator placements to reduce the design space. This, combined with the unknown actuation magnitudes to achieve the twisted shape, means it is not possible to exhaustively search the design space or even use the GA to obtain an optimal actuation configuration. Instead, we select actuated folds by the magnitude of rotation they require, starting with the most rotated fold followed by the second most and so on. For example, if we wish to actuate 20% of the 60 folds in a 5×5 Miura-ori sheet then the 12 folds with the highest required rotation will be actuated.

The first question to consider is that if every fold is actuated by its rotation in the twisted sheet in Figure 8a, will it deform to the same shape? For a rigid-foldable deployment it is implicit that this is true; however, for the twisted sheet the facet deformations are a crucial component of the deformed shape, and these will depend on the input actuation. Results show that the folds must be actuated over 50% further to reach a minimum error in the principal curvatures in the target shape; see Figure 9. Further inspection of Figure 8a shows that significant rotation is limited to a relatively small number of folds, with the rest having a comparatively negligible magnitude. This leads to the second question: what if only a subset of most-rotated folds are ac-

Table 1: Sensitivity analysis of constraint parameter p and how that changes the accuracy of a GA repeated 100 times. The number of times the GA returns the known optimal result and the maximum error in the result of any GA result are considered for all actuator combinations as well as only symmetric combinations

		All Combinations		Symmetric Combinations		
Minimisation Target	p	% Optimal	Max. % error	% Optimal	Max. % error	Symmetric % Penalty
No. of Actuators (ψ)	5	74	6.7	89	6.7	0
	10	100	0	100	0	0
	25	98	9.8	100	0	0
Actuation Energy (ψ)	5	94	0.81	100	0	0.21
	10	92	0.66	95	0.12	0.49
	25	85	2.1	63	0.65	0.21
No. of Actuators (β)	5	27	71	81	68	0
	10	77	0.42	96	0.11	0.29
	25	62	0.98	76	2.3	0
Actuation Energy (β)	5	2	27	25	21	5.14
	10	98	0.37	97	0.35	0.063
	25	87	0.54	94	0.54	0

tuated? Sorting the folds by their magnitude of rotation and actuating the top 40%, leaving the remainder free to act as torsional springs, still shows a response which is similar to simply actuating all of the folds; even actuating only 20% results in a shape approximating the target. These are shown by the grey lines in Figure 9. An explanation lies in the observation that many of the folds do not need to rotate far to reach the desired shape; therefore, as the actuation applied to one of the more highly rotated folds decays [9] before reaching these less rotated folds, much of the desired rotation is already achieved. Lastly, we note that all combinations of actuators in the 5×5 morphing Miura-ori sheet result in a non-zero minimum error due to facet deformations differing between the twisted target sheet and the one actuated by fold rotations. This suggests that, despite clearly approaching an approximation of the target shape, a more refined approach that considers the optimisation of sequencing and individual magnitudes of fold rotations would be necessary to perfectly replicate it.

An alternative approach is to design a rigid-foldable pattern which deploys from a flat sheet to the target three-dimensional twisted shape, such that the facets no longer need to deform to achieve the target shape. First, a smooth version of the target surface, a second order polynomial surface fitted to the lower vertices of the target sheet, is defined. Next, using this fitted surface as the target and the planar 5×5 Miura-ori pattern in Figure 8a as a starting configuration, a rigid-foldable pattern is calculated using the methodology outlined by Hu *et al.* [35]. Lastly, the kinematics of the new rigid-foldable twisting pattern is calculated using the method by Lang & Howell [36]. This helps to define the starting condition prior to actuation and the rotation required on each fold to reach the target shape. This starting condition is defined as kinematically 5% of the way from a flat sheet to the target twisted configuration at the dark blue fold in the bottom left of Figure 8b, therefore avoiding potential bifurcations around the unfolded state. The rigid-foldable twisting pattern, and the magnitude of rotations on the folds required to get from the initial condition to the target shape, is shown in Figure 8b.

As the pattern is rigid-foldable, actuating all folds results in zero error with respect to the target surface at the expected fold rotation; see the darkest blue line in Figure 9. However, if only a subset of folds with largest rotations are actuated in the rigid-foldable twisting pattern, the minimum error increases rapidly compared to the morphing Miura-ori pattern. Contrasting Figures 8a and 8b reveals the cause of this sensitivity to the number of actuators: all of the folds require a significant rotation to transition from flat to the three-dimensional twisted shape. This means that any decay of the input of an actuator has a more significant impact on the final shape achieved in the rigid-foldable twisting pattern.

Extracting the elastic strain energy from the FE models shows that the rigid-foldable twisting pattern requires significantly more energy to reach its target shape; see Table 2. This is the result of the larger fold rotations compared to the morphing Miura-ori pattern. As both patterns originate from different initial states, the magnitudes of energy should not be compared directly; nonetheless, insight can be gained from the effect of additional actuators on the folding energy in the

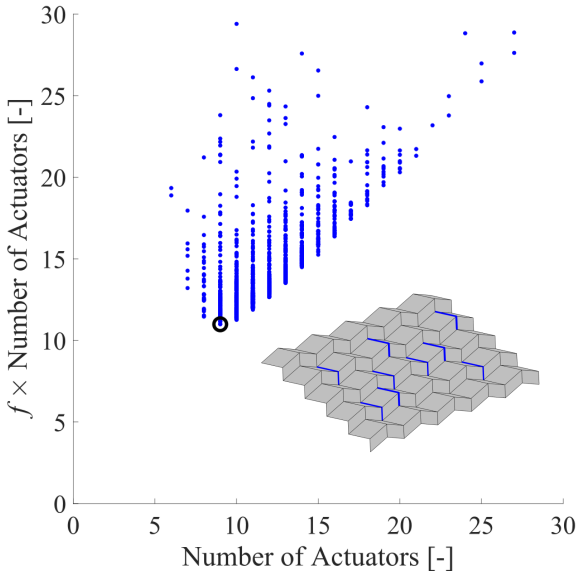

Fig. 7: Every design considered by the GA when minimising the number of actuators required to deploy a 5×5 Miura-ori sheet. A GA is required here as the potential actuation combinations of a 5×5 Miura-ori sheet is nine orders of magnitude higher than that of a 3×3 Miura-ori sheet, and the FEA model has almost twice as many elements, which significantly increases the computational cost. Inset is the resulting optimal combination of actuators

two patterns. For the morphing Miura-ori pattern the energy requirement does not vary considerably with the number of actuators, provided that more than 20% of the folds are actuated, which correlates well with the relatively small changes in error in Figure 9. Again, this is because almost all fold rotation is limited to a small subset of folds, and actuating the other folds, with only a small amount of rotation, therefore does not require much additional energy. Furthermore, the amount of strain energy in the folds and facets is of similar magnitude, which reflects the non-rigid-foldable nature of the deformation. In contrast, the actuation of additional folds in the rigid-foldable twisting pattern requires additional energy, because every fold must undergo significant rotation to reach the target.

Perhaps surprisingly, a rigid-foldable pattern is not necessarily the best approach to transform an origami structure between two configurations. The single-DOF deformation path minimises facet bending, but the larger fold rotations might demand a larger number of actuators as well as greater input energy compared to a morphing pattern. Furthermore, the rigid-foldable pattern is only optimised for a single shape change compared to the flexibility offered by a morphing origami sheet which could follow a non-rigid folding path to a wide variety of potential shapes. The ability to morph from a range of partly-deployed states also provides additional opportunity to reduce the number of actuators or energy required to deform to the desired target shape. We recognise

Table 2: Strain energy at the minimum error configurations in Figure 9, separated into fold and facet components

No. Folds Actuated [%]	Fold Strain Energy [mJ]	Facet Strain Energy [mJ]
Morphing Miura-ori pattern		
20	2.14	2.96
40	1.82	2.55
60	1.66	2.42
80	1.59	2.43
100	1.51	2.40
Rigid-Foldable Twisting Pattern		
20	86.7	24.9
40	113	20.5
60	140	12.8
80	183	8.92
100	189	0.00

that some conclusions are specific to the chosen material system, as higher facet bending and lower fold stiffness would tend to favour a rigid-foldable solution as facet strain energy becomes more dominant in the morphing Miura-ori pattern. Therefore, both the structural design and the actuation design methodology presented in this paper must be used together to effectively design a high performing origami-inspired deployable or morphing system.

5 Conclusions

In order to exploit the potential of origami structures to transform between different shapes, a distributed network of embedded actuators is proposed. Such embedded actuation would enable both deployment (following rigid-origami kinematics) and morphing (also involving facet deformations) of an origami structure. The objective is to minimise the number of actuators and/or their energy requirements for the desired change in geometry.

To assess the performance of the shape transformation, a method for tracking the deformed shape of an origami structure throughout its motion is required. A triangulated surface is defined using the top or bottom vertices of the origami pattern. At the vertices where the triangles meet, the principal curvatures are determined using discrete differential geometry and are compared to a target surface. This method, which is agnostic to rigid body motions, is robust in tracking the deformed shape of both deploying and morphing origami structures.

First, the deployment of a Miura-ori sheet was investigated. The total number of possible combinations of ac-

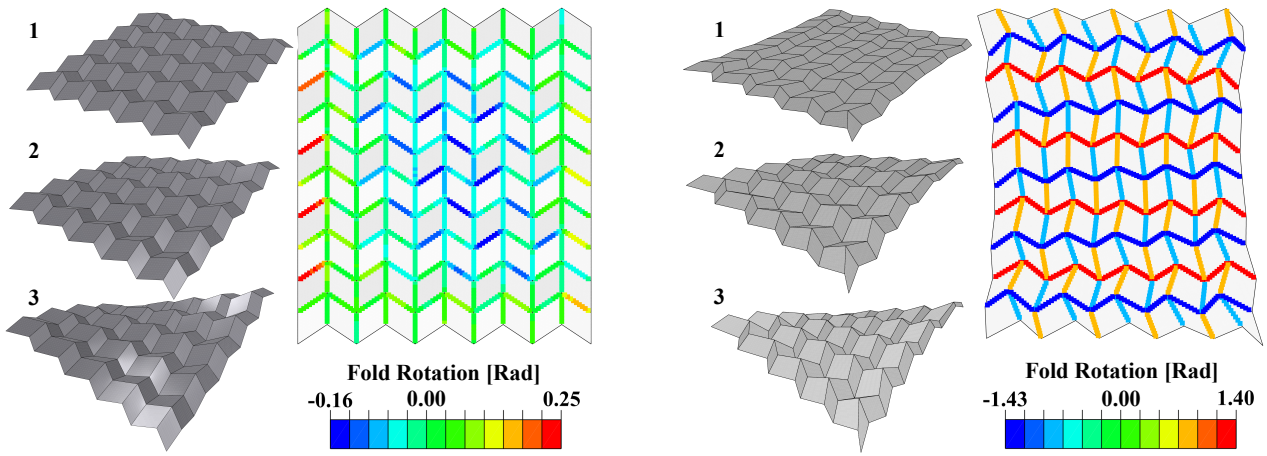

(a) (b)

Fig. 8: The change in fold angle when twisting (a) a partially-folded planar Miura-ori sheet and (b) a pattern designed to rigidly fold from flat to the twisted shape. Images from the beginning, middle, and end of the deformation are labelled 1, 2, and 3 respectively

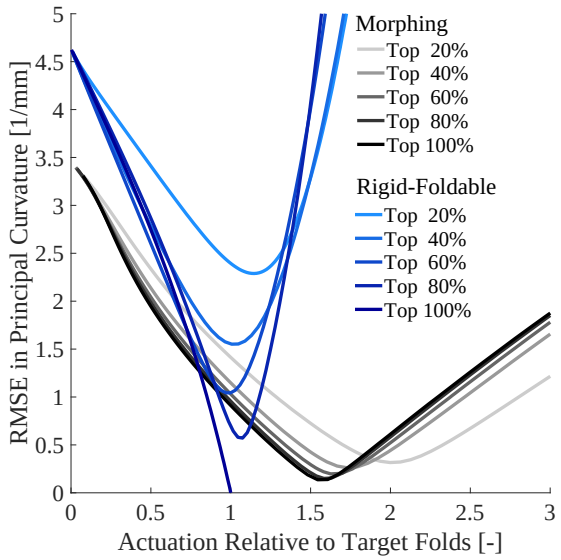

Fig. 9: The error in the first principal curvature when actuating increasing numbers of folds, starting with the folds requiring most rotation. The starting error in the morphing and the rigid-foldable patterns differ because they have different initial states; the morphing Miura-ori pattern is in a partially folded and untwisted state, whereas the rigid-foldable pattern starts from a nominally flat sheet

tuated folds in even relatively small systems rapidly makes an exhaustive search for the optimal actuator combination prohibitively computationally expensive. A 3×3 Miura-ori sheet where actuated folds are paired up at each vertex is used as a suitably reduced design space for this exhaustive search. This is used to verify the use of a Genetic Algorithm (GA) which allows for the investigation of larger sheets, up to five unit cells in either direction.

Second, the non-rigid foldable twisting of a Miura-ori sheet was investigated. As each fold in the twisted sheet is no longer simply a binary 'to actuate or not to actuate' decision, but now could take any range of magnitude of rotation, the potential design space of actuation is increased yet further. Therefore, an alternative method of selecting the actuated folds is used. The magnitude of fold rotations in the twisted shape is recorded, and their relative magnitude guides the selection of actuated folds: the folds requiring most rotation are actuated first. This less computationally intensive approach gives a good approximation of the target shape with only approximately 40% of the folds actuated.

A common school of thought is that the best origami pattern to achieve a certain target shape is one that is rigid foldable, thereby minimising the facet deformations required [3,29,35]. By comparing the actuation of a morphing Miura-ori sheet targeting a twisted shape to one designed to be rigidly foldable from flat to the same twisted shape, we show this does not minimise either the quantity of actuators or the actuation energy required. However, selecting different material for the origami structure could lead to different conclusions on the efficiency of actuating rigid-foldable patterns, as higher facet bending and lower fold stiffness could result in rigid-foldable patterns to be better performing. This reinforces the principle that the design of the pattern, materials, and actuation system cannot be decoupled when designing active origami systems.

Future work on the actuation of origami should address some of the remaining challenges, including the sequencing of actuation and adequately exploring the exponentially increasing design space of larger structures. Furthermore, physical implementation of embedded actuation should be improved before such designs can be used in engineering

systems. Nonetheless, the presented methodology for selecting candidate actuation configurations and assessing their performance compared to a target geometry provides a starting point for the design of truly reconfigurable origami structures.

Acknowledgements

The authors wish to thank Isaac Chenchiah (University of Bristol) for suggesting curvature to characterise an origami shape. This work was supported by the Engineering and Physical Sciences Research Council (EPSRC) through the ACCIS Doctoral Training Centre [grant number EP/G036772/1]. This work was carried out using the computational facilities of the Advanced Computing Research Centre, University of Bristol. Data are available at the University of Bristol data repository, data.bris, at `https://doi.org/10.5523/bris.3gzjg4hdyg4te2t5148ulmh5a7`.

References

[1] Miura, K., 1985. Method of Packaging and Deployment of Large Membranes in Space. Tech. rep., The Institute of Space and Astronautical Science.

[2] Kuribayashi, K., Tsuchiya, K., You, Z., Tomus, D., Umemoto, M., Ito, T., and Sasaki, M., 2006. "Self-deployable origami stent grafts as a biomedical application of Ni-rich TiNi shape memory alloy foil". *Materials Science and Engineering: A,* **419**(1-2), mar, pp. 131–137.

[3] Dudte, L. H., Vouga, E., Tachi, T., and Mahadevan, L., 2016. "Programming curvature using origami tessellations". *Nature Materials,* **15**(5), jan, pp. 583–588.

[4] Tolley, M. T., Felton, S. M., Miyashita, S., Aukes, D., Rus, D., and Wood, R. J., 2014. "Self-folding origami: shape memory composites activated by uniform heating". *Smart Materials and Structures,* **23**(9), p. 094006.

[5] Peraza Hernandez, E. A., Hartl, D. J., and Lagoudas, D. C., 2016. "Design of Origami Structures With Smooth Folds". In Volume 2: Modeling, Simulation and Control; Bio-Inspired Smart Materials and Systems; Energy Harvesting, ASME, p. V002T03A018.

[6] Tachi, T., 2009. "Simulation of Rigid Origami". In *Origami 4*. A K Peters/CRC Press, aug, pp. 175–187.

[7] Morgan, J., Magleby, S. P., and Howell, L. L., 2016. "An Approach to Designing Origami-Adapted Aerospace Mechanisms". *Journal of Mechanical Design,* **138**(5), may, p. 052301.

[8] He, Z., and Guest, S. D., 2020. "On rigid origami II: quadrilateral creased papers". *Proceedings of the Royal Society A: Mathematical, Physical and Engineering Sciences,* **476**(2237), may, p. 20200020.

[9] Grey, S. W., Scarpa, F., and Schenk, M., 2019. "Strain Reversal in Actuated Origami Structures". *Physical Review Letters,* **123**(2), jul, p. 025501.

[10] Silverberg, J. L., Evans, A. A., McLeod, L., Hayward, R. C., Hull, T., Santangelo, C. D., and Cohen, I., 2014. "Using origami design principles to fold reprogrammable mechanical metamaterials". *Science,* **345**(6197), aug, pp. 647–650.

[11] Zhao, Y., Endo, Y., Kanamori, Y., and Mitani, J., 2018. "Approximating 3D surfaces using generalized waterbomb tessellations". *Journal of Computational Design and Engineering,* **5**(4), oct, pp. 442–448.

[12] Hawkes, E., An, B., Benbernou, N. M., Tanaka, H., Kim, S., Demaine, E. D., Rus, D., and Wood, R. J., 2010. "Programmable matter by folding". *Proceedings of the National Academy of Sciences,* **107**(28), pp. 12441–12445.

[13] Lee, K., Wang, Y., and Zheng, C., 2020. "TWISTER Hand: Underactuated Robotic Gripper Inspired by Origami Twisted Tower". *IEEE Transactions on Robotics,* **PP**, pp. 1–13.

[14] Zhang, W., Ahmed, S., Masters, S., Ounaies, Z., and Frecker, M., 2017. "Finite element analysis of electroactive polymer and magnetoactive elastomer based actuation for origami folding". *Smart Materials and Structures,* **26**(10).

[15] Koh, J.-s., Kim, S.-r., and Cho, K.-j., 2014. "Self-Folding Origami Using Torsion Shape Memory Alloy Wire Actuators". In Volume 5B: 38th Mechanisms and Robotics Conference, Vol. 34822, ASME, p. V05BT08A043.

[16] Peraza-Hernandez, E., Hartl, D., Galvan, E., and Malak, R., 2013. "Design and Optimization of a Shape Memory Alloy-Based Self-Folding Sheet". *Journal of Mechanical Design,* **135**(11), oct, p. 111007.

[17] Schenk, M., and Guest, S. D., 2011. "Origami Folding: A Structural Engineering Approach". In Origami 5: Fifth International Meeting of Origami Science, Mathematics, and Education, pp. 291–304.

[18] Evans, A. A., Silverberg, J. L., and Santangelo, C. D., 2015. "Lattice mechanics of origami tessellations". *Physical Review E,* **92**(1), jul, p. 013205.

[19] Santangelo, C. D., 2017. "Extreme Mechanics: Self-Folding Origami". *Annual Review of Condensed Matter Physics,* **8**(1), mar, pp. 165–183.

[20] Nassar, H., Lebée, A., and Monasse, L., 2017. "Curvature, metric and parametrization of origami tessellations: theory and application to the eggbox pattern". *Proceedings of the Royal Society A: Mathematical, Physical and Engineering Sciences,* **473**(2197), jan, p. 20160705.

[21] Wei, Z. Y., Guo, Z. V., Dudte, L., Liang, H. Y., and Mahadevan, L., 2013. "Geometric Mechanics of Periodic Pleated Origami". *Physical Review Letters,* **110**(21), may, p. 215501.

[22] Schenk, M., and Guest, S. D., 2013. "Geometry of Miura-folded metamaterials". *Proceedings of the National Academy of Sciences,* **110**(9), feb, pp. 3276–3281.

[23] Meyer, M., Desbrun, M., Schröder, P., and Barr, A. H., 2003. "Discrete Differential-Geometry Operators for Triangulated 2-Manifolds". In *Visualization and Mathematics III*, Vol. 81. Springer, Berlin, Heidelberg, oct,

pp. 35–57.

[24] Bowen, L., Springsteen, K., Frecker, M., and Simpson, T., 2016. "Trade Space Exploration of Magnetically Actuated Origami Mechanisms". *Journal of Mechanisms and Robotics,* **8**(3), p. 31012.

[25] Fuchi, K., Buskohl, P. R., Bazzan, G., Durstock, M. F., Reich, G. W., Vaia, R. A., and Joo, J. J., 2016. "Design Optimization Challenges of Origami-Based Mechanisms With Sequenced Folding". *Journal of Mechanisms and Robotics,* **8**(5), p. 051011.

[26] Chen, T., Bilal, O. R., Lang, R., Daraio, C., and Shea, K., 2018. "Autonomous Deployment of a Solar Panel Using an Elastic Origami and Distributed Shape Memory Polymer Actuators". *Physical Review Applied,* **10**(1), p. 1.

[27] Mulford, R. B., Jones, M. R., and Iverson, B. D., 2015. "Dynamic Control of Radiative Surface Properties With Origami-Inspired Design". *Journal of Heat Transfer,* **138**(3), p. 032701.

[28] Kilian, M., Monszpart, A., and Mitra, N. J., 2017. "String Actuated Curved Folded Surfaces". *ACM Transactions on Graphics,* **36**(3), pp. 1–13.

[29] He, Z., and Guest, S. D., 2018. "Approximating a Target Surface with 1-DOF Rigid Origami". In *Origami 7*. may.

[30] Cai, J., Ren, Z., Ding, Y., Deng, X., Xu, Y., and Feng, J., 2017. "Deployment simulation of foldable origami membrane structures". *Aerospace Science and Technology,* **67**, pp. 343–353.

[31] Lebée, A., Monasse, L., and Nassar, H., 2018. "Fitting surfaces with the Miura tessellation". In *7OSME*.

[32] Fuchi, K., Buskohl, P. R., Bazzan, G., Durstock, M. F., Reich, G. W., Vaia, R. A., and Joo, J. J., 2015. "Origami Actuator Design and Networking Through Crease Topology Optimization". *Journal of Mechanical Design,* **137**(9), p. 091401.

[33] Gillman, A. S., Fuchi, K., and Buskohl, P. R., 2019. "Discovering Sequenced Origami Folding Through Nonlinear Mechanics and Topology Optimization". *Journal of Mechanical Design,* **141**(4), jan, p. 041401.

[34] The MathWorks Inc., Accessed on: 16/06/2020. "MATLAB Global Optimization Toolbox". `https://uk.mathworks.com/help/gads/index.html`.

[35] Hu, Y., Zhou, Y., and Liang, H., 2020. "Rigid-foldable generalized miura-ori tessellations for three-dimensional curved surfaces". *arXiv:2006.04070*.

[36] Lang, R. J., and Howell, L., 2018. "Rigidly foldable quadrilateral meshes from angle arrays". *Journal of Mechanisms and Robotics,* **10**(2), pp. 1–11.